NANO LETTERS

Letter

pubs.acs.org/NanoLett

Structure of Methylammonium Lead Iodide Within Mesoporous Titanium Dioxide: Active Material in High-Performance Perovskite Solar Cells

Joshua J. Choi,[†,∥] Xiaohao Yang,[‡,∥] Zachariah M. Norman,[†] Simon J. L. Billinge,*[,‡,§] and Jonathan S. Owen*[,†]

[†]Department of Chemistry and [‡]Department of Applied Physics and Applied Mathematics, Columbia University, New York, New York 10027, United States

[§]Condensed Matter Physics and Materials Science Department, Brookhaven National Laboratory, Upton, New York 11973, United States

Supporting Information

ABSTRACT: We report the structure of methylammonium lead(II) iodide perovskite in mesoporous TiO_2, as used in high-performance solar cells. Pair distribution function analysis of X-ray scattering reveals a two component nanostructure: one component with medium range crystalline order (30 atom %) and another with only local structural coherence (70 atom %). The nanostructuring correlates with a blueshift of the absorption onset and increases the photoluminescence. Our findings underscore the importance of fully characterizing and controlling the structure for improved solar cell efficiency.

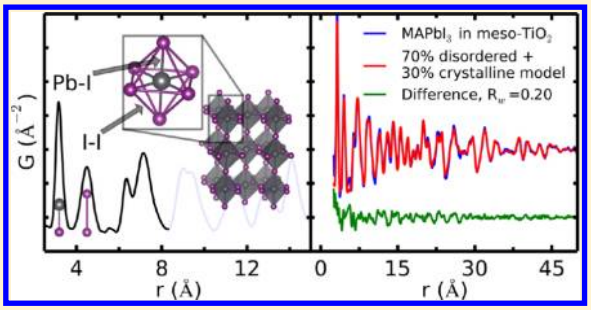

KEYWORDS: *Metal−organic perovskite, structure, pair distribution function, X-ray diffraction, disordered structures*

There has been a strikingly rapid increase in the performance of methylammonium lead iodide ($MAPbI_3$) perovskite solar cells after the first report by Miyasaka and co-workers in 2009;[1] two recent studies, one of which using mixed iodide and chloride, have achieved greater than 15% power conversion efficiency.[2,3] $MAPbI_3$ has a favorable bandgap for photovoltaic applications (1.55 eV) and a large exctinction coefficient.[4−6] Its solution processability and the initial reports of stability under operation[2,7,8] combined with the earth abundance of the constituent materials,[9] make the lead halide perovskites among the most promising solar cell materials.

A full understanding of these devices requires an atomic level understanding of the optically active material. However, this is a major challenge because the active metal−organic perovskite is nanostructured and integrated into a mesoporous network of titania[1,2,7,8,10−17] or alumina[7,12,15] where the majority of the material present is the matrix oxide. It is notoriously difficult to determine the structure of nanomaterials in general, which are not amenable to crystallographic methods,[18] but even more so when they are minority phases in a heterogeneous complex as in this case. Here we report the first fully quantitative structural characterization of mesoporous titania supported $MAPbI_3$[1,7,10,12−14,16] using atomic pair distribution function (PDF) analysis of high energy X-ray diffraction data.[19]

Most of the high efficiency solar cells to date deposit $MAPbI_3$ precursors from solution onto a mesoporous TiO_2 film, crystallizing the perovskite within the tens of nanometer scale pores in the TiO_2 matrix upon removing the solvent.[1,2,7,8,10−17] Early work[1] suggests that the reaction product has the tetragonal perovskite structure[20] due to the observation of Bragg-like peaks in the X-ray diffraction (XRD).[1] Nanoparticles of ∼2 nm were also observed in scanning electron microscopy (SEM) images[1] though such small nanoparticles cannot diffract with any sharp Bragg-like peaks[21,22] and their structure remains in question. Later studies report a similar, qualitative, analysis of $MAPbI_3$ within mesoporous TiO_2 using electron microscopy and XRD,[2,8,10,16,23] though no quantitative structural refinement of the oxide supported perovskite has been reported.

A more quantitative assessment of the structure is important for a number of reasons. First, there are other stable and metastable forms such as two-dimensional (2D) and one-dimensional (1D) structures based on the perovskite motif that may be present in the active layer.[4,5,24−26] Second, the photoluminescent properties of these materials are thought to depend sensitively on the degree of structural order and the presence of defects.[2,6,16] For example, Kanatzidis and co-workers reported that $MAPbI_3$ synthesized by grinding lead iodide and methylammonium iodide powder shows stronger photoluminescence compared to samples slowly crystallized from solution,[6] though no detailed structural explanation was presented. In the context of solar cells, different deposition and processing methods result in vastly different device perform-

Received: September 19, 2013
Revised: November 12, 2013
Published: November 22, 2013

   dx.doi.org/10.1021/nl403514x | *Nano Lett.* 2014, 14, 127−133

ances but the structural origin of these differences is not known.[2,3,12,16,27,28] A record efficiency device reported by the Grätzel group was fabricated via "sequential deposition" of lead iodide and methylammonium iodide and it is not obvious what structural changes are caused by this processing.[2] Last, it is suggested that[1,10,23] small nanoparticles observed in these devices are important to the device performance and optical properties, yet these nanostructures remain uncharacterized.

To address these issues we turned to atomic PDF methods that yield quantitative information about structure on the nanoscale[19,21,29−33] and can differentiate competing structural models.[34] These methods are powerful in the current case where nanostructure is superimposed on a much stronger signal from the oxide matrix support.[35−37] We applied PDF methods to study samples of $MAPbI_3$ that were synthesized in an identical manner to those used in high-efficiency solar cells.[1,2,7,8,10−17] The PDF method analyzes the total scattering where all structure-relevant scattering is used, including Bragg and diffuse scattering over a wide range of reciprocal space. It directly provides atom-to-atom distances in the material on length-scales from a few angstroms to tens of nanometers. For example, the first and second peak in the PDF of $MAPbI_3$ corresponds to the nearest (Pb−I) and second nearest distances (I−I) respectively (Figure 1a). While the peak positions in the PDF directly yield bond length information, the peak areas contain information about coordination numbers and abundance within the sample. In addition, rich information about the material's vibrational structure, bond stiffness, strain, and distortion can be directly extracted by examining the peak width and shape.[19] In general, a highly ordered structure gives sharp PDF peaks, while a disordered structure results in broad or diminished PDF peaks. Importantly, PDF enables the characterization of structures without long-range order;[29] it has been successfully applied to amorphous and liquid materials for decades[38,39] and recently has been widely used for studying nanoparticles and other nanostructured materials.[21,22,30,32,40−54]

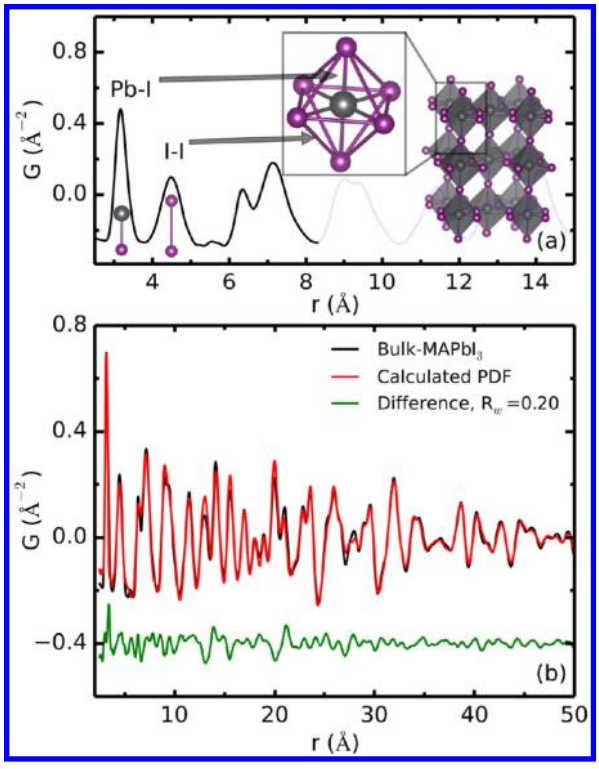

Figure 1. (a) A PDF of bulk $MAPbI_3$ perovskite. The first peak corresponds to the nearest neighbor distance (Pb−I), the second peak the shortest I−I distance, and so on. (b) PDFs from bulk-$MAPbI_3$ (black) and the best-fit model (red) with the difference curve offset below (green). The experimental PDF from the highly crystalline reference perovskite sample shows a good match (R_w = 0.20) with the simulated PDF of the tetragonal structure (space group *I4cm*) (see inset in panel a and the main text for details).

In this work, we confirm that crystallites of $MAPbI_3$ form a tetragonal perovskite phase within the mesoporous TiO_2 matrix, which give rise to the previously observed XRD patterns.[1,2,8,10,16] However, we find that nearly 70% of the $MAPbI_3$ exists in a disordered state with a very short structural coherence length of 1.4 nm. We associate this component with the small nanoparticles previously observed in electron microscopy.[1,10,23] We present quantitative structural information on this disordered component. Intriguingly, the presence of disordered $MAPbI_3$ correlates with strong changes in photoluminescence (PL) and absorbance spectra compared to the spectra of highly crystalline $MAPbI_3$. Our findings suggest that a varying amount of disordered nanocrystalline material may cause differences in solar cell performance seen with different processing methods reported recently,[2,3,27,28] which underscores the importance of a full structural characterization of these devices.

All perovskite samples were prepared following literature methods[1,7,10,11,13,14,16] (see Supporting Information for more details). Briefly, $MAPbI_3$ perovskite embedded in mesoporous TiO_2 was prepared by spin-casting a solution of PbI_2 and CH_3NH_3I (1:1 mol ratio) in γ-butyrolactone onto a mesoporous TiO_2 film, which was then annealed at 100 °C for 30 min. Dozens of such thin films were prepared, gently scraped off the substrate, and packed into kapton capillaries and sealed prior to PDF measurements. As a reference sample, crystalline $MAPbI_3$ (bulk-$MAPbI_3$) was prepared by removing the γ-butyrolactone solvent from the $MAPbI_3$ solution at 100 °C under vacuum. X-ray powder diffraction experiments were performed at the X17A beamline at the National Synchrotron Light Source at Brookhaven National Laboratory (see Supporting Information for experimental details). High-energy (67.577 keV) X-rays were used to obtain PDFs with high resolution using the rapid acquisition PDF mode[55] that utilizes planar detectors. The data were reduced to 1D powder patterns using SrXplanar[56] and transformed to obtain the PDF using the PDFgetX3 program.[57] Structural modeling was carried out using the SrFit program[58] (see Supporting Information).

For reference, we first consider the raw XRD pattern of bulk crystalline $MAPbI_3$ (Supporting Information Figure S1). Scherrer grain size analysis shows that the bulk-$MAPbI_3$ sample is a polycrystalline mixture with an average grain size larger than 50 nm, beyond the spectral resolution of the measurement (Supporting Information). A PDF extracted from the XRD data shows excellent agreement with a simulated PDF based on the tetragonal perovskite structure (space group *I4cm*) reported in the literature for single crystal $MAPbI_3$ at room temperature[6] (Figure 1b). A structural model was refined to the data that is within 0.3% of the lattice parameters reported by Poglitsch (Table 1).[20]

The PDF from $MAPbI_3$ embedded in mesoporous TiO_2 is shown in Figure 2a and compared with the PDF from a sample of pure mesoporous TiO_2. The PDF signal from the perovskite/TiO_2 composite is dominated by the signal from TiO_2, despite the greater scattering cross section of lead and

dx.doi.org/10.1021/nl403514x | Nano Lett. 2014, 14, 127−133

Table 1. Structural Parameters Obtained from the PDF Fitting[a]

	bulk-$MAPbI_3$	meso-$MAPbI_3$ MRO-component	meso-$MAPbI_3$ Nanocomponent
a (Å)	8.886(4)	8.903(4)	9.204(15)
c (Å)	12.643(6)	12.617(12)	12.66(4)
D_n (Å)			13.7(2)
U_{iso}(Pb) (Å^2)	0.0240(4)	0.022(5)	0.037(6)
U_{iso}(I) (Å^2)	0.0465(4)	0.048(2)	0.035(4)
U_{iso}(C) (Å^2)	0.10(3)	0.18(8)	0.18(8)
U_{iso}(N) (Å^2)	0.10(3)	0.04(1)	0.04(1)
x_{I_1}	0.2885	0.280	0.276
z_{I_1}	−0.014	−0.0178	−0.0135
z_{I_2}	0.2449	0.246	0.255
z_{Pb}	−0.002	0.0005	−0.008
z_C	0.340	0.312	0.346
z_N	0.242	0.240	0.241

[a]The structural model has space group *I*4*cm* with Pb, C, N, and two I positions at (0,0, z_{Pb}), (0, 0, z_C), (0, 0, z_N), (x_{I_1}, 0.5-x_{I_1}, z_{I_1}), (0, 0, z_{I_2}), respectively. The model was fit to the bulk-$MAPbI_3$ and the meso-$MAPbI_3$ PDFs. In the latter case, the fit was carried out as a multiphase fit with two components, a medium-range ordered (MRO) and a nanocomponent. D_n is the diameter of the nanodomain obtained from the PDF refinement.

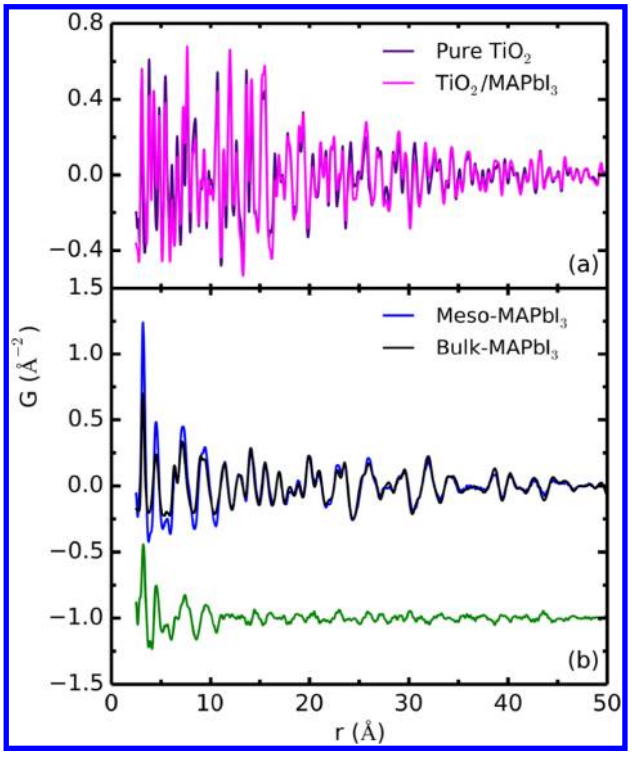

Figure 2. (a) Experimental PDF of pure mesoporous TiO_2 (dark violet) and $MAPbI_3$ in mesoporous TiO_2 (magenta). (b) Processed PDF of the meso-$MAPbI_3$ (after TiO_2 signal subtraction) (blue) and the PDF of the bulk-$MAPbI_3$ reference (black) and the difference between the two curves (green).

iodine, and indicates that the perovskite is a minor component. To extract the signal from $MAPbI_3$, a careful subtraction of the TiO_2 background signal was performed by a least-squares regression. A scaling factor for the pure TiO_2 PDF signal was adjusted and then subtracted from the composite signal. The resulting difference is taken to be the signal from $MAPbI_3$ (hereafter referred to as meso-$MAPbI_3$), which is shown in Figure 2b overlaid on the PDF of bulk-$MAPbI_3$. It appears as a well-defined signal that is not overly dominated by noise, a result of sufficient collection of X-ray scattering data. The bulk and meso-$MAPbI_3$ curves agree extremely well in the high-*r* region of the PDF, which strongly suggests that the overall structure of the two is the same. However, the intensity of the peaks show very intriguing differences; although the peak positions match the bulk-$MAPbI_3$ pattern well, the meso-$MAPbI_3$ shows much stronger intensity in the <10 Å region compared to the crystalline reference. The difference between these two experimental curves is shown as the green line in Figure 2b. Close inspection of the difference curve indicates that it is similar in structure to the PDF of the reference bulk-$MAPbI_3$ sample, but its amplitude falls off quickly with increasing *r*. This result indicates that the solid is nanostructured with a significant component that has only short-range structural correlations.

We undertook quantitative modeling to learn more about the structure of the meso-$MAPbI_3$ sample (see Supporting Information for details). To assess whether there are contributions from phases other than the tetragonal perovskite structure, we simulated PDFs based on various known crystal structures (Supporting Information Figure S3). As expected, the tetragonal perovskite model provides the best match for the data. On the other hand, simulated PDFs of incorrect structures show peaks in positions that do not agree with the experimental data, indicating where we would expect peaks if other structures are present in smaller quantities.

In principle, there are two scenarios that can explain the higher signal intensity at low-*r* compared with the bulk-$MAPbI_3$ reference sample (Figure 2). First, if the meso-$MAPbI_3$ is composed of nanocrystals their finite size will result in PDF intensity that falls off at high-*r* (see Supporting Information).[19,21] Similarly, the presence of two components can explain the data; a relatively crystalline and well-ordered fraction that accounts for correlations at high-*r* and a second component that is nanocrystalline or highly disordered. We hypothesize that the nanoparticles observed in SEM and transmission electron microscopy images reported previously[1,10,23] are responsible for the disordered component, whereas the ordered component is responsible for the crystalline tetragonal perovskite Bragg peaks seen in XRD signals reported in the same studies.

The single and two-component possibilities can be distinguished by quantitative modeling. First, we tested a single-phase spherical nanoparticle model to fit the meso-$MAPbI_3$ PDF (Supporting Information Figure S3a). The best single phase fit was refined with a nanoparticle diameter of 100 Å, albeit with poor overall agreement (R_w = 0.34). Next we explored the possibility that the meso-$MAPbI_3$ sample consists of two components as discussed above, a medium range ordered perovskite crystallite (MRO-component) and a nanoparticle component with the same base structure but short-range structural coherence (nanocomponent). A linear superposition of the two phases was used, where the range of structural coherence of the nanocomponent and the relative amount of each phase were varied along with the other structural parameters to obtain the best fit to the experimental PDF. The resulting fit is excellent, as shown in Figure 3a with

dx.doi.org/10.1021/nl403514x | *Nano Lett.* 2014, 14, 127−133

an R_w = 0.21 that is comparable in quality to that of the crystalline control sample (Figure 1b). The refined structural parameters are listed in Table 1.

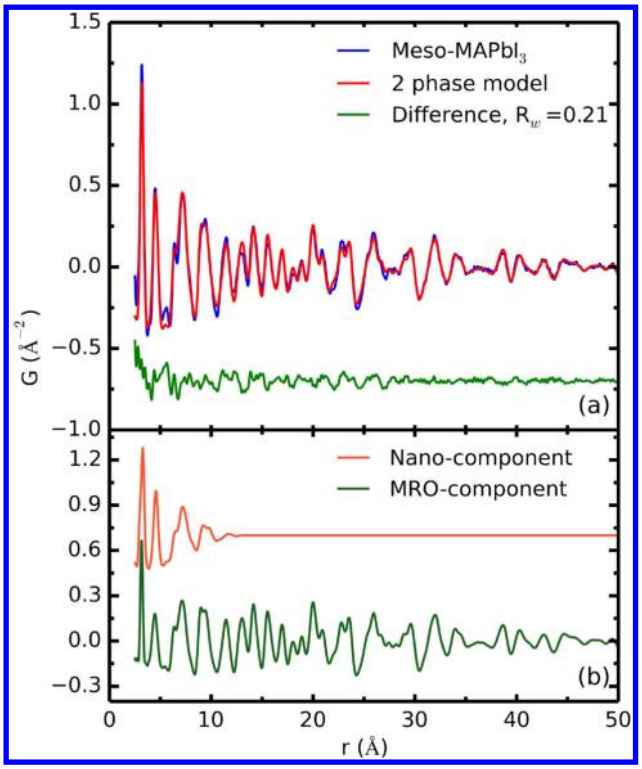

Figure 3. (a) Refinement results of meso-$MAPbI_3$ using two phase model. The experiment PDF (blue) and the fitted PDF (red) are overlaid and the difference curve (green) is offset below. (b) The MRO-component (green) and nanocomponent (orange) of calculated PDF. See in text for detailed description of two phase model.

The refined parameters for the MRO-component are in excellent agreement with those from the crystalline bulk reference sample. We note that because of the limited Q-resolution of our X-ray data, a characteristic of the rapid acquisition PDF method, we can only determine a lower bound of the particle size in the medium-range ordered material to be 10 nm. To estimate the grain size, we turn to the powder diffraction pattern of the meso-$MAPbI_3$ sample, which shows significantly broadened Bragg peaks compared to sharp peaks expected from macroscopic crystals. Scherrer grain size analysis determined the average grain size to be 7.5 nm, assuming a spherical grain shape[59] (Supporting Information). We note that quantitation via Scherrer analysis lacks reliability, especially for a mixture such as this, which contains a significant fraction of 1.4 nm crystallites. However, we can conclude from the broadened Bragg peaks that the grains of the MRO-component are nanoscale. Given the pore size of the mesoporous TiO_2 is 20 nm on average, we expect the grain size of the MRO-component to be bound by this limit. Thus, the $MAPbI_3$ within mesoporous TiO_2 is composed of a mixture of nanometer scale grains with long ($10 < r < 20$ nm) and short (1.4 nm) correlation lengths.

The range of structural coherence in the nanocomponent is very short, 1.4 nm, which is much smaller than the physical dimensions of nanoparticles previously observed in these systems.[1,10,23] If, as we suspect, the nanocomponent signal is coming from nanoparticles in the system, it implies that these particles exhibit significant structural disorder. Also notable is the coherence length of 1.4 nm, which is about the length of two corner-sharing PbI_6 octahedra. On the basis of this information, we can conclude that the structure of the nanocomponent is likely composed of very small nanoparticles or a material composed of clusters of two to eight octahedral lead iodide building blocks that only maintain nearest neighbor order.[60]

The proportion of nanocomponent refined in the fits is very large, ~70%. This result is striking as it indicates that the majority of the $MAPbI_3$ material in mesoporous TiO_2 is significantly disordered, a structural feature that would have been undetected by conventional XRD techniques employed in previous studies. This nanostructure is expected to have a significant impact on the optoelectronic properties and device performance of perovskites and further discussion and investigation are needed.

If the PDF signal of the nanocomponent is coming from discrete clusters with 1.4 nm dimensions, they would be composed of only a few corner-sharing PbI_6 octahedra and could have an average lead and iodine ratio significantly different from PbI_3. Likewise, in the analogous 1D or 2D perovskite structures ($[(CH_3NH_3)_2(PbI_4)]_n$ and $[(CH_3NH_3)_3(PbI_5)]_n$), the ratio of lead and iodine differs significantly from the nominal PbI_3 stoichiometry. To test whether there is evidence for a significant deviation of stoichiometry from PbI_3, we performed elemental analysis using energy dispersive X-ray spectroscopy (EDS). These measurements showed an iodine to lead ratio of 3.01 ± 0.15 (see Supporting Information) and not a higher value expected from pervoskites with lower dimensionality.[4] Further, the selective formation of structures with iodine to lead ratios higher than the ratio present in the deposition solution requires that lead iodide is formed as a byproduct and this is not seen in the experimental PDF data (Supporting Information Figures S4 and S5). Thus, the nanocomponent is consistent with the formula of $MAPbI_3$ but is significantly structurally disordered.

We next turned to the optical absorption and photoluminescence (PL) spectra of the $MAPbI_3/TiO_2$ composite to further probe the nanoparticulate perovskite. The absorptance spectrum of the composite is shown in Figure 4 overlaid with that of the crystalline bulk-$MAPbI_3$ reference. The spectrum of

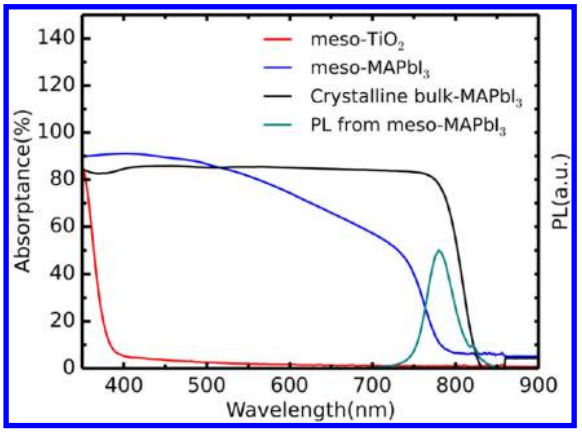

Figure 4. Absorptance spectra of bulk crystalline $MAPbI_3$ (black), meso-$MAPbI_3$ (blue), and mesoporous TiO_2 (red) samples. Photoluminescence spectrum of meso-$MAPbI_3$ (cyan). No photoluminescence was detected from the bulk crystalline $MAPbI_3$ sample.

dx.doi.org/10.1021/nl403514x | Nano Lett. 2014, 14, 127−133

the bulk-$MAPbI_3$ is very similar to one reported previously,[61] while the spectrum of the composite sample is clearly different. The absorption onset of the composite is blue shifted by ~50 meV and is more gradual compared to the bulk perovskite. In addition, there are several broad features while the optical response of the crystalline reference is flat. We note that most of the reported absorption spectra of $MAPbI_3/TiO_2$ composites employed in high-performance solar cells show similar features,[2,10,16] as do spin coated thin films without a mesoporous oxide matrix.[62,63] Thus far, an adequate explanation is lacking.

Our observation of highly disordered material in the PDF can help explain the blue shifted and somewhat featured absorption spectrum. However, the PDF simulations and Scherrer grain size analysis indicate that at least 30% of the material (MRO-component) is composed of crystallites larger than the exciton Bohr diameter (4−6 nm)[64,65] and quantum confinement alone cannot explain these results. Likewise, the lower dielectric environment of the porous composite sample can only partially explain the blueshift; from calculations[64] on a $MAPbI_3$ particle of 10 nm diameter in air, the maximum shift in the absorption onset due to the dielectric medium is estimated to be less than 30 meV or roughly half the observed shift (Supporting Information). Thus the blueshift appears to be a characteristic of the band structure of the particular form of the $MAPbI_3$ found in mesoporous TiO_2, rather than a consequence of the dielectric medium or the grain size. We speculate that defects are present in the MRO-component that cause the blueshift. Such defects appear reasonable given the relatively large proportion of the disordered nanocomponent formed under these conditions. For example, a structure with methylammonium iodide and lead iodide vacancies can alter both the electronic structure as well as the dielectric constant by changing the number of polarizable lead−iodine bonds and is consistent with the PDF signals from the MRO-component.[66]

Another interesting difference is the photoluminescence signal from the composite material. While, the PL spectrum of meso-$MAPbI_3$ shows a peak at higher energy (780 nm) than the bulk-$MAPbI_3$ absorption edge, no PL could be detected from the crystalline bulk-$MAPbI_3$ sample. Thus disordered $MAPbI_3$ is photoluminescent, while crystalline material is not. Previous studies report similar observations; Kanatzidis and co-workers observed significantly brighter PL from $MAPbI_3$ samples that were synthesized by grinding a mixture of powdered lead iodide and methylammonium iodide at room temperature, rather than crystallizing the perovskite from homogeneous solution.[6] Similarly, Grätzel and co-workers use a decrease in PL during the formation of $MAPbI_3$ to monitor the crystallization process.[2] Spin coated thin $MAPbI_3$ films without a mesoporous titanium dioxide matrix that display a blue shifted absorption onset[62,63] as well as those crystallized within mesoporous Al_2O_3 (Supporting Information) are photoluminescent. Finally, these absorptance and PL features are distinct from previously reported spectra of layered 2D perovskites, which show sharp excitonic absorption features at 510 nm and a PL signal at 525 nm.[4,5,67] Together these results indicate that the PL is related to the blue shifted absorption onset and is not likely caused by an interfacial effect, like an interaction with the mesoporous oxide support, or the presence of another perovskite phase.[6]

Previous studies have measured an exciton binding energy in $MAPbI_3$ slightly higher than thermal energy at room temperature (35−50 meV).[64,65] Thus, in bulk $MAPbI_3$ crystals dissociation of excitons into free carriers can inhibit radiative recombination at room temperature. However, in a defected solid where confinement and dielectric effects cause a blueshift of the absorption onset the exciton binding energy will increase, thereby favoring radiative recombination. A recent study made a similar proposal to explain the temperature dependence of $MAPbI_3$ photoluminescence.[68] Although the complete lack of luminescence from the bulk $MAPbI_3$ sample remains to be explained, the increased radiative recombination probability of the nanostructured material is consistent with the changes to the absorption onset and the nanostructuring observed with PDF.[2,6,16] These observations point to the important influence of fabrication methods on structure and its role in the generation of excited carriers and thereby the photovoltaic efficiency.[2,3,12,16,27,28]

In conclusion, we report the structure of the active $MAPbI_3$ layer within a mesoporous matrix of TiO_2 that is utilized in high-performance perovskite-based solar cells.[1,2,7,8,10−17] Approximately 30% of the material consists of a medium-range ordered tetragonal perovskite structure, while 70% of the material forms as a highly disordered phase with local perovskite structure extending over a range of only ~1.4 nm. The mesoporous TiO_2 support controls the nanostructure by confining the grains to the dimensions of the pores. Further, we demonstrate that nanostructuring influences the optical properties and propose that defects within $MAPbI_3$ cause an optical blue shift and the observed PL. These findings suggest that disordered and amorphous phases, which are not visible in conventional XRD measurements, are likely important to device efficiency, a factor that will depend on the processing method.[2,3,27,28] These findings underscore the importance of fully characterizing and controlling the crystallinity in these devices.

■ ASSOCIATED CONTENT

Supporting Information

Information on materials, sample synthesis methods, PDF data processing and analysis, optical spectroscopy, scanning electron microscopy and energy-dispersive X-ray spectroscopy, and Scherrer grain size analysis of WAXS data. This material is available free of charge via the Internet at http://pubs.acs.org.

■ AUTHOR INFORMATION

Corresponding Authors

*E-mail: (J.S.O.) jso2115@columbia.edu.
*E-mail: (S.J.L.B.) sb2896@columbia.edu.

Author Contributions

‖J.J.C. and X.Y. contributed equally.

Notes

The authors declare no competing financial interest.

■ ACKNOWLEDGMENTS

We thank Dr. Abraham Wolcott for critical reading of the manuscript. This work was supported by the Center for Re-Defining Photovoltaic Efficiency Through Molecule Scale Control, an Energy Frontier Research Center funded by the U.S. Department of Energy, Office of Science, Office of Basic Energy Sciences under Award Number DE-SC0001085. X-ray experiments were carried out at the National Synchrotron Light Source, Brookhaven National Laboratory, which is supported by the U.S. Department of Energy, Division of Materials

Sciences and Division of Chemical Sciences, DE-AC02-98CH10886.

REFERENCES

(1) Kojima, A.; Teshima, K.; Shirai, Y.; Miyasaka, T. *J. Am. Chem. Soc.* **2009**, *131*, 6050−6051.
(2) Burschka, J.; Pellet, N.; Moon, S.-J.; Humphry-Baker, R.; Gao, P.; Nazeeruddin, M. K.; Grätzel, M. *Nature* **2013**, *499*, 316−319.
(3) Liu, M.; Johnston, M. B.; Snaith, H. J. *Nature* **2013**, *501*, 395−398.
(4) Mitzi, D. B. Synthesis, Structure, and Properties of Organic-Inorganic Perovskites and Related Materials. In *Progress in Inorganic Chemistry*; Karlin, K. D., Ed.; John Wiley & Sons, Inc.: 2007; pp 1−121.
(5) Papavassiliou, G. C. *Mol. Cryst. Liq. Cryst. Sci. Technol., Sect. A* **1996**, *286*, 231−238.
(6) Stoumpos, C. C.; Malliakas, C. D.; Kanatzidis, M. G. *Inorg. Chem.* **2013**, *52*, 9019−9038.
(7) Kim, H.-S.; Lee, C.-R.; Im, J.-H.; Lee, K.-B.; Moehl, T.; Marchioro, A.; Moon, S.-J.; Humphry-Baker, R.; Yum, J.-H.; Moser, J. E.; Grätzel, M.; Park, N.-G. *Sci. Rep.* **2012**, *2*, 591.
(8) Noh, J. H.; Im, S. H.; Heo, J. H.; Mandal, T. N.; Seok, S. I. *Nano Lett.* **2013**, *13*, 1764−1769.
(9) Wadia, C.; Alivisatos, A. P.; Kammen, D. M. *Environ. Sci. Technol.* **2009**, *43*, 2072−2077.
(10) Im, J.-H.; Lee, C.-R.; Lee, J.-W.; Park, S.-W.; Park, N.-G. *Nanoscale* **2011**, *3*, 4088−4093.
(11) Etgar, L.; Gao, P.; Xue, Z.; Peng, Q.; Chandiran, A. K.; Liu, B.; Nazeeruddin, M. K.; Grätzel, M. *J. Am. Chem. Soc.* **2012**, *134*, 17396−17399.
(12) Lee, M. M.; Teuscher, J.; Miyasaka, T.; Murakami, T. N.; Snaith, H. J. *Science* **2012**, *338*, 643−647.
(13) Abrusci, A.; Stranks, S. D.; Docampo, P.; Yip, H.-L.; Jen, A. K. Y.; Snaith, H. J. *Nano Lett.* **2013**, *13*, 3124−3128.
(14) Bi, D.; Yang, L.; Boschloo, G.; Hagfeldt, A.; Johansson, E. M. J. *J. Phys. Chem. Lett.* **2013**, *4*, 1532−1536.
(15) Edri, E.; Kirmayer, S.; Cahen, D.; Hodes, G. *J. Phys. Chem. Lett.* **2013**, *4*, 897−902.
(16) Heo, J. H.; Im, S. H.; Noh, J. H.; Mandal, T. N.; Lim, C.-S.; Chang, J. A.; Lee, Y. H.; Kim, H.-j.; Sarkar, A.; Nazeeruddin, M. K.; Grätzel, M.; Seok, S. I. *Nat. Photonics* **2013**, *7*, 486−491.
(17) Zhao, Y.; Zhu, K. *J. Phys. Chem. Lett.* **2013**, *4*, 2880−2884.
(18) Billinge, S. J. L.; Levin, I. *Science* **2007**, *316*, 561−565.
(19) Egami, T.; Billinge, S. J. L. *Underneath the Bragg Peaks: Structural Analysis of Complex Materials*, 2nd ed.; Pergamon: Amsterdam, 2013.
(20) Poglitsch, A.; Weber, D. *J. Chem. Phys.* **1987**, *87*, 6373.
(21) Masadeh, A. S.; Božin, E. S.; Farrow, C. L.; Paglia, G.; Juhas, P.; Billinge, S. J. L.; Karkamkar, A.; Kanatzidis, M. G. *Phys. Rev. B* **2007**, *76*, 115413.
(22) Yang, X.; Masadeh, A. S.; McBride, J. R.; Božin, E. S.; Rosenthal, S. J.; Billinge, S. J. L. *Phys. Chem. Chem. Phys.* **2013**, *15*, 8480−8486.
(23) Kim, H.-S.; Lee, J.-W.; Yantara, N.; Boix, P. P.; Kulkarni, S. A.; Mhaisalkar, S.; Grätzel, M.; Park, N.-G. *Nano Lett.* **2013**, *13*, 2412−2417.
(24) Arend, H.; Huber, W.; Mischgofsky, F. H.; Richter-Van Leeuwen, G. K. *J. Cryst. Growth* **1978**, *43*, 213−223.
(25) Mitzi, D. B.; Feild, C. A.; Harrison, W. T. A.; Guloy, A. M. *Nature* **1994**, *369*, 467−469.
(26) Mitzi, D. B.; Wang, S.; Feild, C. A.; Chess, C. A.; Guloy, A. M. *Science* **1995**, *267*, 1473−1476.
(27) Eperon, G. E.; Burlakov, V. M.; Docampo, P.; Goriely, A.; Snaith, H. J. *Adv. Funct. Mater.* **2013**, DOI: 10.1002/adfm.201302090.
(28) Jeng, J.-Y.; Chiang, Y.-F.; Lee, M.-H.; Peng, S.-R.; Guo, T.-F.; Chen, P.; Wen, T.-C. *Adv. Mater.* **2013**, *25*, 3727−3732.
(29) Billinge, S. J. L. *J. Solid State Chem.* **2008**, *181*, 1695−1700.
(30) Gilbert, B.; Huang, F.; Zhang, H.; Waychunas, G. A.; Banfield, J. F. *Science* **2004**, *305*, 651−654.
(31) I. Korsunskiy, V.; Neder, R. B.; Hofmann, A.; Dembski, S.; Graf, C.; Rühl, E. *J. Appl. Crystallogr.* **2007**, *40*, 975−985.
(32) Page, K.; Proffen, T.; Niederberger, M.; Seshadri, R. *Chem. Mater.* **2010**, *22*, 4386−4391.
(33) Proffen, T.; Billinge, S. J. L.; Egami, T.; Louca, D. *Z. Kristallogr.* **2003**, *218*, 132−143.
(34) Petkov, V.; Billinge, S. J. L.; Larson, P.; Mahanti, S. D.; Vogt, T.; Rangan, K. K.; Kanatzidis, M. G. *Phys. Rev. B* **2002**, *65*, 092105.
(35) Chapman, K. W.; Chupas, P. J.; Kepert, C. J. *J. Am. Chem. Soc.* **2005**, *127*, 11232−11233.
(36) Petkov, V.; Billinge, S. J. L.; Vogt, T.; Ichimura, A. S.; Dye, J. L. *Phys. Rev. Lett.* **2002**, *89*, 075502.
(37) Shatnawi, M.; Paglia, G.; Dye, J. L.; Cram, K. C.; Lefenfeld, M.; Billinge, S. J. L. *J. Am. Chem. Soc.* **2007**, *129*, 1386−1392.
(38) Warren, B. E. *X-ray Diffraction*; Courier Dover Publications: Mineola, NY, 1969; p 402.
(39) Wright, A. C. *Glass Phys. Chem.* **1998**, *24*, 148.
(40) Božin, E. S.; Chatterji, T.; Billinge, S. J. L. *Phys. Rev. B* **2012**, *86*, 094110.
(41) Božin, E. S.; Schmidt, M.; DeConinck, A. J.; Paglia, G.; Mitchell, J. F.; Chatterji, T.; Radaelli, P. G.; Proffen, T.; Billinge, S. J. L. *Phys. Rev. Lett.* **2007**, *98*, 137203.
(42) Chupas, P. J.; Chapman, K. W.; Jennings, G.; Lee, P. L.; Grey, C. P. *J. Am. Chem. Soc.* **2007**, *129*, 13822−13824.
(43) Cliffe, M. J.; Dove, M. T.; Drabold, D. A.; Goodwin, A. L. *Phys. Rev. Lett.* **2010**, *104*, 125501.
(44) Cossairt, B. M.; Juhas, P.; Billinge, S. J. L.; Owen, J. S. *J. Phys. Chem. Lett.* **2011**, *2*, 3075−3080.
(45) Dmowski, W.; Yin, H.; Dai, S.; Overbury, S. H.; Egami, T. *J. Phys. Chem. C* **2010**, *114*, 6983−6988.
(46) Du, P.; Kokhan, O.; Chapman, K. W.; Chupas, P. J.; Tiede, D. M. *J. Am. Chem. Soc.* **2012**, *134*, 11096−11099.
(47) Farrow, C. L.; Bediako, D. K.; Surendranath, Y.; Nocera, D. G.; Billinge, S. J. L. *J. Am. Chem. Soc.* **2013**, *135*, 6403−6406.
(48) Greedan, J. E.; Derakhshan, S.; Ramezanipour, F.; Siewenie, J.; Proffen, T. *J. Phys.: Condens. Matter* **2011**, *23*, 164213.
(49) Kim, H.; Nakamura, J.; Shao, H.; Nakamura, Y.; Akiba, E.; Chapman, K. W.; Chupas, P. J.; Proffen, T. *J. Phys. Chem. C* **2011**, *115*, 7723−7728.
(50) Lazarević, N.; Abeykoon, M.; Stephens, P. W.; Lei, H.; Bozin, E. S.; Petrovic, C.; Popović, Z. V. *Phys. Rev. B* **2012**, *86*, 054503.
(51) Li, W.; Harrington, R.; Tang, Y.; Kubicki, J. D.; Aryanpour, M.; Reeder, R. J.; Parise, J. B.; Phillips, B. L. *Environ. Sci. Technol.* **2011**, *45*, 9687−9692.
(52) Martin, C. D.; Antao, S. M.; Chupas, P. J.; Lee, P. L.; Shastri, S. D.; Parise, J. B. *Appl. Phys. Lett.* **2005**, *86*, 061910.
(53) Neilson, J. R.; Kurzman, J. A.; Seshadri, R.; Morse, D. E. *Chem.—Eur. J.* **2010**, *16*, 9998−10006.
(54) Paglia, G.; Božin, E. S.; Billinge, S. J. L. *Chem. Mater.* **2006**, *18*, 3242−3248.
(55) Chupas, P. J.; Qiu, X.; Hanson, J. C.; Lee, P. L.; Grey, C. P.; Billinge, S. J. L. *J. Appl. Crystallogr.* **2003**, *36*, 1342−1347.
(56) Yang, X.; Juhas, P.; Billinge, S. J. L. *Estimating statistical uncertainties on powder diffraction and small angle scattering data from 2-D planar X-ray detectors*; arXiv:1309.3614; 2013.
(57) Juhás, P.; Davis, T.; Farrow, C. L.; Billinge, S. J. L. *J. Appl. Crystallogr.* **2013**, *46*, 560−566.
(58) Farrow, C. L.; Juhás, P.; Billinge, S. J. L. SrFit., unpublished.
(59) Smilgies, D.-M. *J. Appl. Crystallogr.* **2009**, *42*, 1030−1034.
(60) Davis, T.; Johnson, M.; Billinge, S. J. L. *Cryst. Growth Des.* **2013**, *13*, 4239−4244.
(61) Baikie, T.; Fang, Y.; Kadro, J. M.; Schreyer, M.; Wei, F.; Mhaisalkar, S. G.; Graetzel, M.; White, T. J. *J. Mater. Chem. A* **2013**, *1*, 5628−5641.
(62) Stranks, S. D.; Eperon, G. E.; Grancini, G.; Menelaou, C.; Alcocer, M. J. P.; Leijtens, T.; Herz, L. M.; Petrozza, A.; Snaith, H. J. *Science* **2013**, *342*, 341−344.
(63) Xing, G.; Mathews, N.; Sun, S.; Lim, S. S.; Lam, Y. M.; Grätzel, M.; Mhaisalkar, S.; Sum, T. C. *Science* **2013**, *342*, 344−347.

(64) Hirasawa, M.; Ishihara, T.; Goto, T.; Uchida, K.; Miura, N. *Phys. B: Condens. Matter* **1994**, *201*, 427−430.
(65) Tanaka, K.; Takahashi, T.; Ban, T.; Kondo, T.; Uchida, K.; Miura, N. *Solid State Commun.* **2003**, *127*, 619−623.
(66) Delerue, C.; Lannoo, M.; Allan, G. *Phys. Rev. B* **2003**, *68*, 115411.
(67) Papavassiliou, G. C.; Patsis, A. P.; Lagouvardos, D. J.; Koutselas, I. B. *Synth. Met.* **1993**, *57*, 3889−3894.
(68) Zhang, W.; Saliba, M.; Stranks, S. D.; Sun, Y.; Shi, X.; Wiesner, U.; Snaith, H. J. *Nano Lett.* **2013**, *13*, 4505−4510.

dx.doi.org/10.1021/nl403514x | *Nano Lett.* 2014, 14, 127−133